Developmental Cognitive Neuroscience 45 (2020) 100853

Contents lists available at ScienceDirect

Developmental Cognitive Neuroscience

journal homepage: www.elsevier.com/locate/dcn

Longitudinal patterns of white matter fibre density and morphology in children are associated with age and pubertal stage

Sila Genc [a,b,c,*], Charles B. Malpas [b,d], Alisha Gulenc [e], Emma Sciberras [c,e,f], Daryl Efron [e,g], Timothy J. Silk [b,f,1], Marc L. Seal [b,c,1]

[a] Cardiff University Brain Research Imaging Centre (CUBRIC), Cardiff University, Cardiff, UK
[b] Developmental Imaging, Murdoch Children's Research Institute, Parkville, Australia
[c] Department of Paediatrics, University of Melbourne, Parkville, Australia
[d] Clinical Outcomes Research Unit (CORe), Department of Medicine, Royal Melbourne Hospital, University of Melbourne, Parkville, Australia
[e] Population Health, Murdoch Children's Research Institute, Parkville, Australia
[f] School of Psychology, Deakin University, Geelong, Australia
[g] The Royal Children's Hospital, Parkville, Australia

ARTICLE INFO

Keywords:
White matter
Longitudinal
Fixel-based analysis
Puberty
Fibre density
Fibre morphology

ABSTRACT

The pubertal period involves dynamic white matter development. This period also corresponds with rapid gains in higher cognitive functions including attention, as well as increased risk of developing mental health difficulties. This longitudinal study comprised children aged 9–13 years (n = 130). Diffusion magnetic resonance imaging (dMRI) data were acquired (b = 2800s/mm^2, 60 directions) at two time-points. We derived measures of fibre density and morphology using the fixel-based analysis framework and performed a tract-based mixed-effects modelling analysis to understand patterns of white matter development with respect to age, sex, pubertal stage, and the change in pubertal stage. We observed significant increases in apparent fibre density across a large number of white matter pathways, including major association and commissural pathways. We observed a linear relationship between pubertal stage and fibre density and morphology in the right superior longitudinal fasciculus, and fibre morphology in the right inferior longitudinal fasciculus. Finally, we report a significant interaction between the change in pubertal stage and age in the development of fibre density, for left-lateralised association tracts. Overall, white matter development across ages 9–13 years involves the expansion of major white matter fibre pathways, with key association pathways linked with pubertal stage.

1. Introduction

Puberty is a critical period of development, marking the transition from childhood to reproductive maturity (Dorn et al., 2006). Brain structure is particularly sensitive to remodelling with exposure to pubertal hormones (Juraska and Willing, 2017). Previous diffusion tensor imaging (DTI) studies have shown a strong link between advancing pubertal stage and greater white matter microstructural organisation (Ladouceur et al., 2012; Herting et al., 2012, 2017).

World-wide, the peak age of onset of psychiatric disorders is age 14 years (Kessler et al., 2005). The presence of internalising problems, including anxiety and depression, during this sensitive period of development pose risk for later case-level disorder (Shankman et al., 2009). Whether puberty influences the onset of mental health problems and neurodevelopmental pathways, or vice versa, is not well understood. What is clear, however, is that these interrelated factors can alter the structural and functional reorganisation of the brain (Paus et al., 2008). Alongside internalising problems, externalising disorders can co-exist

Abbreviations: ADHD, attention-deficit/hyperactivity disorder; CCG, cingulum cingulate gyrus; CCH, cingulum hippocampus; CSD, constrained spherical deconvolution; CST, cortico-spinal tract; FA, fractional anisotropy; FBA, fixel-based analysis; FC, fibre cross-section; FD, fibre density; FDC, fibre density and cross-section; FOD, fibre orientation distribution; Fmajor, forceps major; Fminor, forceps minor; Fx, fornix; IFOF, inferior fronto-occipital fasciculus; ILF, inferior longitudinal fasciculus; MRI, magnetic resonance imaging; NICAP, Neuroimaging of the Children's Attention Project; PDS, pubertal development scale; SEIFA, Socio-Economic Indexes for Areas; SES, socio-economic status; SLF, superior longitudinal fasciculus; UF, uncinate fasciculus.

* Corresponding author at: Cardiff University Brain Research Imaging Centre (CUBRIC), Cardiff University, Cardiff, CF24 4HQ, UK.
E-mail address: gencs@cardiff.ac.uk (S. Genc).

[1] Equal senior author.

https://doi.org/10.1016/j.dcn.2020.100853
Received 3 May 2019; Received in revised form 31 July 2020; Accepted 24 August 2020
Available online 28 August 2020

with commonly occurring disorders in childhood, such as Attention-Deficit/Hyperactivity Disorder (ADHD) (Polanczyk et al., 2007). Whilst ADHD symptoms often present before pubertal onset, these symptoms can become more severe during the transition to adolescence, whereby increases in attentional difficulties and externalising symptoms can alter neuropsychological function (Langberg et al., 2008).

Recent advances in diffusion magnetic resonance imaging (dMRI) models facilitate the investigation of links between physical and behavioural phenotypes with brain development on a magnified neurobiological scale (Tamnes et al., 2017). The recently introduced fixel-based analysis (FBA) framework (Raffelt et al., 2017) and subsequent longitudinal modifications to this (Genc et al., 2018), allow the quantification of white matter fibre properties such as fibre density and morphology (see Box 1 for detailed interpretations). The primary measure of apparent fibre density (FD) reflects the total intra-axonal signal fraction per fibre pathway. The measure of fibre morphology encompasses both fibre cross-section (FC) and fibre-density and cross-section (FDC). FC is sensitive to macroscopic changes in the cross-sectional area perpendicular to a fibre bundle experienced during registration to a template image. FDC incorporates features of FD and FC, and acts as a surrogate marker of alterations to the capacity for information transfer across a fibre bundle.

Compared to commonly used DTI metrics such as FA or mean diffusivity (MD), fixel-based FD is a stronger candidate for signifying microstructural organisation (Kelley et al., 2019), as it is both sensitive (at high b-values) to the intra-axonal signal (Genc et al., 2020), and specific to fibre populations (Raffelt et al., 2015). By comparison, FA measurements can be conflated by crossing fibres and extra-axonal signal contamination (Jones et al., 2013; Bach et al., 2014; Beaulieu, 2009), making biophysical interpretations challenging. With the use of robust neuroimaging studies using high-quality dMRI data, it is possible to unravel the specific neurobiological links between brain structure and developmental factors during this sensitive period of growth (Pines et al., 2020).

In this study, we investigate developmental patterns of age, sex and puberty with respect to white matter fibre density and morphology in commonly investigated white matter tracts. We hypothesise that fibre

Box 1
Interpretation of fixel-based metrics.

Measure	Micro/macro?	Interpretation
Fibre Density (FD)	Microscopic density	A microscopic estimate of the density of axons* within a particular fibre population in a given voxel. An increase in FD could result from developmental processes, such as growth in axon diameter, or increase in the number of axons occupying a given space, whereas a decrease in fibre density could be due to a loss of axons, such as in neurodegeneration.
Fibre Cross-section (FC)	Macroscopic morphology	A morphological measure of the macroscopic change in cross-sectional area perpendicular to a fibre bundle experienced during registration to a template image. Increases in FC could reflect expansion of a fibre bundle via increased extra-cellular space, myelination, or both.
Fibre Density and Cross-section (FDC)	Microscopic and macroscopic effects	A combined measure that incorporates both the microscopic and macroscopic effects described above, thus providing sensitivity to any differences related to the capacity of the white matter to transmit information. Increases in FDC highlight this increased capacity to transmit information.

Note: See Raffelt et al. (2017) for complete descriptions of these measures. *The interpretation of these measures as related to the microstructure of 'axons' depends on the strength of the diffusion weighting (Genc et al., 2020).

density and morphology follow the typical course of white matter development previously shown with DTI. We expect that advanced dMRI measures will provide finer insights into associations with sex and puberty development of micro- and macro-structure. We then evaluate whether the longitudinal change in fibre density is associated with the change in pubertal stage and age. In order to understand these complex associations, we combine a tract-based approach with mixed-effects modelling upon a cohort of children with and without attentional difficulties.

2. Methods

2.1. Participants

This study reports on a sample of children aged 9–13 years recruited as part of the Neuroimaging of the Children's Attention Project study (NICAP; see Silk et al. (2016) for a detailed protocol). This longitudinal study was approved by The Royal Children's Hospital Melbourne Human Research Ethics Committee (HREC #34,071). Briefly, children were initially recruited at 7 years of age as part of the Children's Attention Project (CAP) study (Sciberras et al., 2013) from 43 socio-economically diverse primary schools distributed across the Melbourne metropolitan area, Victoria, Australia. Children underwent comprehensive assessment for ADHD at age 7 via the Diagnostic Interview Schedule for Children (DISC-IV) completed with parents face-to-face. Children were categorised as either meeting a negative or positive diagnosis for ADHD. A subsample of children from the CAP study, which either met or did not meet criteria for ADHD, were invited to participate in the neuroimaging study NICAP at age 10 (Fig. S1).

At 10 years of age, children and their primary caregiver were invited for a 3.5 -h appointment at The Melbourne Children's campus, which included a child assessment, parent questionnaire, mock scan, and MRI scan. Direct assessments and MRI scans were performed by a trained research assistant who was blind to the child's diagnostic status. Children were invited for a follow-up appointment approximately 16 months following their initial visit (M = 16.14, SD = 2.37 months). Overall, only data from children imaged at both imaging time-points: time-point 1 (age: M = 10.4, SD = .44 years old) and time-point 2 (age: M = 11.7, SD = .51 years old), were included for analysis in the current study.

Written informed consent was obtained from the parent/guardian of all children enrolled in the study. Children were excluded from the study if they had a neurological disorder, intellectual disability, or serious medical condition (e.g. diabetes, kidney disease).

2.2. Measures

The following measures were obtained at both imaging time-points. General intellectual ability was estimated using the Wechsler Abbreviated Scale of Intelligence (WASI) matrix reasoning sub-test (Wechsler, 1999). The Connors 3 ADHD Index (10-items) was administered via parent survey (Conners et al., 2011), in order to capture the variation in ADHD symptom severity across time-points. The Strengths and Difficulties Questionnaire (SDQ) was administered in the form of a parent survey as a measure of emotional/behavioural difficulties (Goodman, 1997). Using the responses from this questionnaire, the scores derived from the peer problems and emotional problems scales were added to generate a combined internalising difficulties score, and the scores from the hyperactivity and conduct scales were added to generate a combined externalising difficulties score (Goodman et al., 2010). The Pubertal Development Scale questionnaire (PDS; Petersen et al. (1988) was administered to parents, and a total PDS score (PDSS) combining features of adrenarche and gonadarche was computed for each imaging time-point (PDSS; Shirtcliff et al. (2009)). Additional information on the psychometric properties of these measures are summarised in Supplementary Information.

Child height and weight were measured using the average of two consecutive measurements to calculate a Body-Mass index (BMI) (kg/m^2). Socio-economic status (SES) was determined using the Socio-Economic Indexes for Areas (SEIFA), based on Australian Census data.

2.3. Image acquisition and pre-processing

Diffusion MRI data were acquired at two distinct time-points on a 3.0 T Siemens Tim Trio, at The Melbourne Children's Campus, Parkville, Australia. Data were acquired using the following protocol: b = 2800s/mm^2, 60 directions, 4 volumes without diffusion weighting, 2.4 × 2.4 × 2.4 mm voxel size, echo-time / repetition time (TE/TR) = 110/3200 ms, multi-band acceleration factor of 3, acquisition matrix = 110 × 100, bandwidth =1758 Hz. A total of 152 participants had longitudinal MRI data. Of those, 130 participants had useable diffusion MRI data, therefore the subsequent image processing and analysis was performed on these 130 participants with imaging data at two time-points (Fig. S1).

All dMRI data were processed using MRtrix3 (v3.0RC3; Tournier et al. (2019)) using pre-processing steps from a recommended fixel-based analysis (FBA) pipeline (Raffelt et al., 2017). For each scan, these pre-processing steps were: denoising (Veraart et al., 2016); eddy, motion, and susceptibility induced distortion correction (Andersson and Sotiropoulos, 2016); bias field correction (Tustison et al., 2010); and group-wise intensity normalisation. Data were then upsampled by a factor of 2, and a fibre-orientation distribution (FOD) was estimated in each voxel. Total intra-cranial volume for each T1-weighted image at each time-point was calculated using FreeSurfer (version 6) (Reuter et al., 2012). Images were visually inspected for motion artefact (assessed by the presence of Venetian blinding artefact), and whole datasets were excluded if excessive motion was present. In addition, we calculated mean frame-wise displacement using the FSL software library (v5.0.10) (Smith et al., 2004).

2.4. Longitudinal template generation

In order to build an unbiased longitudinal template, we selected 40 individuals, with equal numbers of males and females, to first generate intra- subject templates. For each of these individuals, the time-point 1 and time-point 2 FOD maps were transformed to their midway space and subsequently averaged to generate an unbiased intra-subject template. The 40 intra-subject FOD templates were used as input for the population template generation step.

Following generation of the population template, each individual's FOD image was registered to this longitudinal template (Raffelt et al., 2011), and the resulting transformed FOD within each template space voxel segmented to produce a set of discrete fixels. Reorientation of fixel directions due to spatial transformation, correspondence of these fixels with the template image, and derivation of FBA metrics, was performed as described previously (Genc et al., 2018). The output metrics fibre density (FD), fibre cross-section (FC), and fibre density and cross-section (FDC) (in template space) were then subjected to further statistical analysis.

2.5. Tractography

We chose to delineate 7 key bilateral white matter fibre pathways, alongside 3 commissural bundles, which make up the John's Hopkins University (JHU) white matter tractography atlas available in FSL. These pathways were delineated to segment fixels from the whole-brain fixel template which corresponded with our tracts of interest. To aid in the spatial identification of specific fibre bundles, we used a three-step process to improve specificity (Fig. 1), summarised as follows:

- *Atlas registration:* The FA image derived from the JHU-ICBM atlas (Smith et al., 2004) was non-linearly transformed to our population

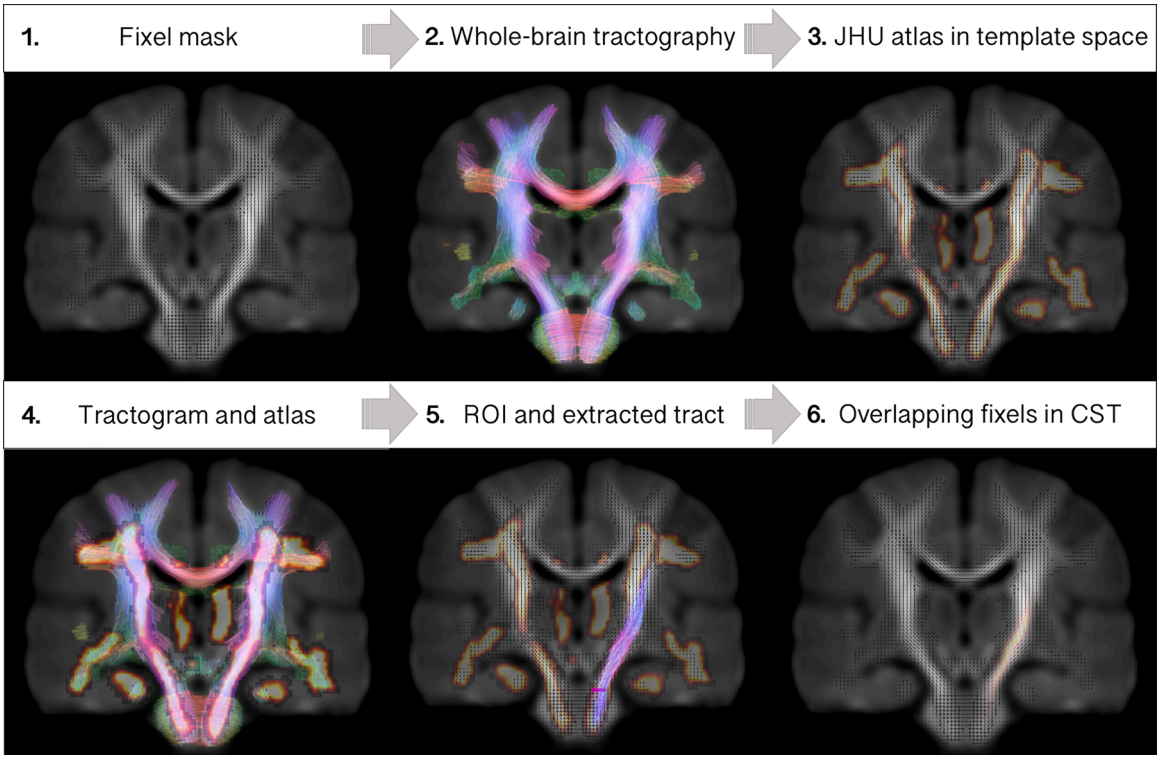

Fig. 1. Protocol for defining fixels overlapping tracts of interest. Example shown is for a single ROI to delineate the left corticospinal tract.

template, and the resulting transformations were applied to warp the JHU tractography atlas to population template space.

- *Whole-brain tractogram overlay:* The whole-brain population-based tractogram was visualised in order to identify specific bundles. This tractogram was visualised as colour-coded directions, to further enable the identification of specific bundles (i.e. corticospinal tract runs inferior to superior, therefore is coloured blue).
- *Region of interest (ROI) selection:* We used a protocol defined in Wakana et al. (2007) to aid in the placement of inclusion ROIs for each major fibre bundle. We placed two separate inclusion ROIs in regions identified in the protocol, making sure they overlapped the JHU tractography atlas and whole brain tractogram. For bilateral tracts, the opposite hemisphere was used as an exclusion ROI. The whole brain tractography map was then edited using *tckedit*, and visualised, to check the anatomical correctness of the tract. In cases where spurious streamlines were present, these were rerun with an additional manually drawn exclusion ROI.

The subsequently generated 17 white matter tracts (Fig. S2), also referred to as regions, were then converted to fixel maps using the whole-brain fixel template (*tck2fixel*), and binarised for statistical sampling of output maps (*mrthreshold*). For each participant at each time-point, we calculated mean FD, FC, and FDC values in each of the fixel masks derived from the 17 white matter tracts for subsequent statistical analyses. An example of these steps for one representative white matter tract can be visualised in Fig. 1.

2.6. Statistical analyses

All statistical analyses were performed within R (version 3.4.3). Data visualisation was performed using *ggplot2* (Wickham, 2016) and *raincloud* tools in R (van Langen, 2020; M et al., 2019). To investigate developmental patterns of FBA metrics across the 17 tracts, we applied linear mixed effects modelling using *lme4* (Bates et al., 2015), a method which allows for hierarchical structures observed in longitudinal data.

The first aim was to describe normative development of white matter fibre properties with respect to age, sex, and pubertal stage (main effects). We built a linear model which included age (linear term) and sex (female as the reference group). For each white matter tract, we compared the fit of this standard model with subsequent models including pubertal stage as a fixed term, and interaction terms including age by pubertal stage, sex by pubertal stage, and age by sex.

$$\begin{aligned} &\text{Level 1}: Y_{ij} = \beta 0_j + \beta 1_j \text{Age}_{ij} + \beta 2_j \text{Sex}_{ij} + \in_{ij} \\ &\text{Level 2}: \beta 0_j = \gamma 00 + u0 \end{aligned} \quad (1)$$

In which Y_{ij} represents the fibre density in each white matter tract at the i'th time-point for the j'th individual. As age is mean centered, the fixed intercept $\gamma 00$ represents the mean fibre density at the mean age of the sample.

The second aim was to assess whether the longitudinal change in white matter fibre properties was associated with the change in pubertal stage, over the two time-points. To do this, we set up a simple linear model with FD at time-point 1, age at time-point 1 (linear term), sex (female as the reference group) and the change in pubertal stage. The difference in age between time-points and pubertal stage at time-point 1 were entered as covariates. For each white matter tract, we compared the fit of this standard model with subsequent models including the change in pubertal stage by sex and the change in pubertal stage by age as interaction terms. Table S1 summarises the formulae for each mixed-effects model tested.

$$\begin{aligned} \Delta Y = {} & \beta 1 \text{FD}_{t1} + \beta 2 \text{Age}_{t1} + \beta 3 \text{Sex} + \beta 4 \Delta \text{PDSS} \\ & + \beta 5 \Delta \text{Age} + \beta 6 \text{PDSS}_{t1} + \epsilon \end{aligned} \quad (2)$$

In which ΔY represents the change in fibre density in each white matter tract, FD is the fibre density and t_1 represents time-point 1.

Finally, we performed an exploratory analysis of the impact of symptom severity on white matter fibre properties (main effects). Our sample was originally selected by dichotomising groups based on ADHD symptom severity. However, rather than dichotomising groups at the extreme ends of mental health and attentional difficulties, we aimed to perform a dimensional analysis to shed light on whether continuous

patterns of behavioural phenotypes relate to white matter fibre properties. We built a linear model (as per model 1) which included age (linear term), sex (female as the reference group) and symptom severity.

For each aim tested, we fitted separate models for each white matter metric (FD, FC, FDC) in each white matter tract and describe the best fitting model in the results section. The most parsimonious model was selected based on lowest Akaike Information Criterion (AIC) values. We computed bootstrapped 95 % confidence intervals (n = 5000 simulations) and report these for each model coefficient as β [95 % CI]. Evidence for an association is represented when confidence intervals do not cross zero. We additionally report p-values, adjusted using False Discovery Rate (FDR) correction (p_{FDR}; Benjamini and Hochberg (1995)).

3. Results

3.1. Participant characteristics

Differences in participant characteristics over the 16-month follow-up period are reported in Table 1 and visualised in Fig. 2. We observed developmental increases in physical characteristics such as BMI and PDSS ($p < .001$), and in WASI matrix reasoning raw score ($p < .001$). Behaviourally, we observed an increase in internalising symptoms ($p < .001$) but no change in externalising symptoms ($p > .05$) assessed by the SDQ. There was some evidence for a decrease in ADHD symptoms over time ($p = .04$).

We assessed whether there was evidence for regional differences in age-related patterns of white matter microstructure (Fig. 3), and associations between our phenotypic variables of interest. We observed a significant region by age interaction, suggesting that region-specific age-related patterns exist. To investigate these region-specific relationships, we computed multiple linear mixed-effects models for each white matter tract. Results from the mixed-effects modelling analysis are presented for each predictor (Table 2; Fig. 3).

3.2. Main effects of age, sex, and pubertal stage

Age related increases in fibre density (FD) over time were localised to the bilateral cingulum cingulate gyrus, bilateral corticospinal tract, forceps major and minor and bilateral superior longitudinal fasciculus. Significant increases in fibre cross-section (FC) were observed in the bilateral cingulum cingulate gyrus, bilateral corticospinal tract, forceps major, fornix, bilateral inferior fronto-occipito fasciculus, and bilateral superior longitudinal fasciculus. Increases in fibre density and cross-section (FDC) were observed in the bilateral cingulum cingulate gyrus, bilateral corticospinal tract, forceps major and minor, fornix, bilateral inferior fronto-occipito fasciculus and bilateral superior longitudinal fasciculus. All regions listed significantly increased in fibre density and morphology over time, and no regions decreased. The longitudinal changes in common fibre pathways changing over time are visualised in Fig. 4.

We observed no significant sex differences in fibre density across any of the regions studied. For the morphological analyses, females had higher FDC than males in the forceps minor, β [95 % CI] = −.46 [−.79, −.13].

We observed a positive relationship between pubertal stage and fibre properties in the right superior longitudinal fasciculus for FD, β [95 % CI] = .12 [.03, .21], FC, β [95 % CI] = .14 [.06, .23], and FDC, β [95 % CI] = .16 [.07, .24], and for the right inferior longitudinal fasciculus for FC, β [95 % CI] = .19 [.08, .30], and FDC, β [95 % CI] = .18 [.07, .30]. These findings are summarised in Fig. 5.

Total intra-cranial volume (TIV) was a significant predictor of FC over all of the white matter tracts studied and FDC for all regions apart from the left cingulum hippocampus.

3.3. Longitudinal change in pubertal stage

We observed no main effect of the change in pubertal stage and the change in white matter microstructure. We observed an interaction between the change in pubertal stage and age at time-point 1, with the longitudinal change in fibre density over time for: the left corticospinal tract, β [95 % CI] = .19 [.04, .35], left inferior fronto-occipital fasciculus, β [95 % CI] = .25 [.07, .42], left inferior longitudinal fasciculus, β [95 % CI] = .19 [.01, .37], and the left uncinate fasciculus, β [95 % CI] = .24 [.06, .42]. For these regions, a larger change in PDSS score combined with older age resulted in a larger increase in fibre density.

3.4. Main effects of symptom severity and impact of motion

The results of the exploratory analysis between symptom severity and white matter microstructure are summarised in Table S3. We observed no significant association between ADHD symptom severity and white matter fibre density, across the 17 tracts studied.

All analyses were rerun with frame-wise displacement included to mitigate any impact of motion on our findings, particularly given the nature of the sample and potential for greater motion artefact in children with attention/hyperactivity phenotypes. The results for the linear mixed-effects models remained unchanged (Tables S2, S3), and we observed no main effect of motion on the models tested for fibre density in each tract. We did observe an effect of motion on the morphological measures (FC and FDC) for some tracts, suggesting that motion artefact can influence the computation of morphological measures, however, this had no bearing on the final results.

4. Discussion

In our longitudinal diffusion MRI study of 130 children aged 9-13 years across two time-points, we identify regional patterns of white matter fibre density and morphology related to age, sex and pubertal

Table 1
Change in participant characteristics over the follow-up interval.

Variable	Time-point 1 M(SD)		Time-point 2 M(SD)		Difference
	Female	Male	Female	Male	*p-value*
Age, years	10.36 (.40)	10.39 (0.46)	11.67 (.44)	11.75 (.55)	*< .001*
Socio-economic status (SES)	1007 (46)	1022 (44)	1007 (46)	1021 (44)	.32
Body Mass Index, kg/m^2	20 (3.5)	19 (3.8)	21 (4.0)	20 (4.3)	*< .001*
Pubertal stage, PDSS	2.0 (.9)	1.2 (.4)	3 (.9)	1.5 (.7)	*< .001*
SDQ internalising	4.8 (4)	4.5 (4)	8.1 (4)	7.4 (3)	*< .001*
SDQ externalising	5.7 (5)	7.7 (5)	5.1 (4)	7.4 (5)	.19
ADHD symptoms	3.8 (6)	7.5 (7)	3.3 (5)	6.9 (7)	.04
Matrix reasoning, raw score	22 (4.7)	23 (4.9)	24 (3.4)	25(4.6)	*< .001*

Difference in participant characteristics between all participants across distinct time-points was calculated using a paired samples *t*-test. Data are further grouped by sex: N(females) = 47; N(males) = 83. M = mean, SD = standard deviation.

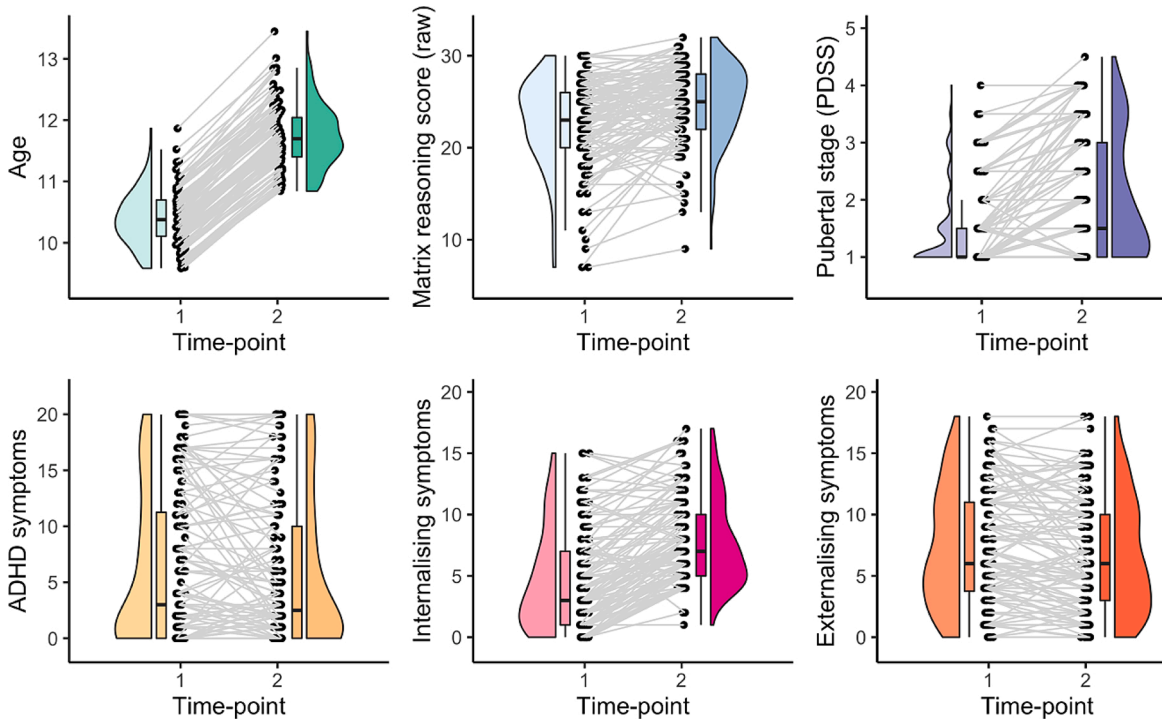

Fig. 2. Change in participant characteristics over the 16-month follow-up period. Longitudinal data points are connected by a line.

development. These findings open up new avenues for investigating the interaction between white matter fibre properties and developmental factors, to unravel multiple contributions to altered neurodevelopmental pathways.

4.1. Main effects of age and sex

We observed age-related development of fibre density in the bilateral cingulum cingulate gyrus, bilateral corticospinal tract, forceps major and minor and bilateral superior longitudinal fasciculus. Similar patterns were observed for fibre cross-section and fibre density and cross-section. The region-specific development we observed is consistent with findings from many diffusion tensor imaging studies (see Tamnes et al. (2018) for a full review) and fixel-based analyses (Genc et al., 2018) in typically developing children of this age range. This may suggest that regional fibre development is consistent in this age range (9–13 years), regardless of variations due to pubertal stage. Regions such as the bilateral cingulum hippocampus, inferior longitudinal fasciculus, and uncinate fasciculus may have delayed maturation, completing maturation closer to the completion of adolescence and early adulthood (Lebel and Beaulieu, 2011).

In terms of sex differences in microstructure, a number of longitudinal developmental studies have also reported no sex differences in white matter development using DTI (Brouwer et al., 2012; Krogsrud et al., 2016; Lebel and Beaulieu, 2011; Tamnes et al., 2010), consistent with our findings. However, some studies of older samples studies have shown that boys have higher FA than girls in a number of associative white matter pathways (Seunarine et al., 2016; Schmithorst et al., 2008; Herting et al., 2012). Given our analyses are focused on data acquired at high diffusion weightings sensitised to the intra-axonal signal, discrepancies in findings could be due to differences in the sensitivity of MRI acquisition and modelling parameters to various neurobiological properties, for example myelin content and extracellular properties.

The sex differences in fibre morphology observed in the forceps minor suggest that females have greater capacity for information transfer across this white matter tract. These differences could plausibly be a signature of anatomical sex differences between males and females, potentially induced by early perinatal exposure to testosterone (Sisk and Foster, 2004). Neuroimaging studies have shown that testosterone and oestradiol impact brain volume across adolescence (Herting et al., 2014). Additionally (or alternatively) these differences could be perpetuated by the onset of pubertal processes and rising hormone levels in females, compared with males, as females generally begin puberty 1–2 years earlier than males (Dorn et al., 2006). Oestrogen receptors exist on oligodendrocytes, which may provide an avenue for myelin production (Zhang et al., 2004). Whilst we have not directly studied myelination in this study, this may be one explanation for the sex differences in fibre morphology observed in anterior and posterior callosal tracts.

4.2. Main effects of pubertal stage

A positive association between pubertal stage and fibre density, fibre cross-section and fibre density and cross-section was observed in the right superior longitudinal fasciculus. This suggests a linear relationship between pubertal development and fibre maturation, likely driven by the expansion of fibre bundles by virtue of axonal growth and myelination. The superior longitudinal fasciculus is a white matter fibre most associated with language ability, semantic memory, and executive function, in developmental and adult populations. It anatomically connects two regions important for language - Broca's and Wernicke's area, and the relationship between language ability and microstructure in the SLF has been extensively reported (Catani et al., 2005). Similarly, we observed that fibre morphology of the right inferior longitudinal fasciculus exhibited a positive relationship with pubertal stage.

The pubertal period involves regulation and remodelling of white matter (Herting et al., 2017, 2012) with rising adrenal and gonadal (Maninger et al., 2009; Perrin et al., 2008; Pesaresi et al., 2015; Pangelinan et al., 2016) hormones. Previous studies have shown puberty-related increases in FA in the right insular gyrus with physical development (Herting et al., 2012) and decreases in MD in the superior and inferior longitudinal fasciculi (Menzies et al., 2015). This is consistent with our findings of a positive relationship between pubertal stage and fibre density and morphology in the right SLF, and fibre

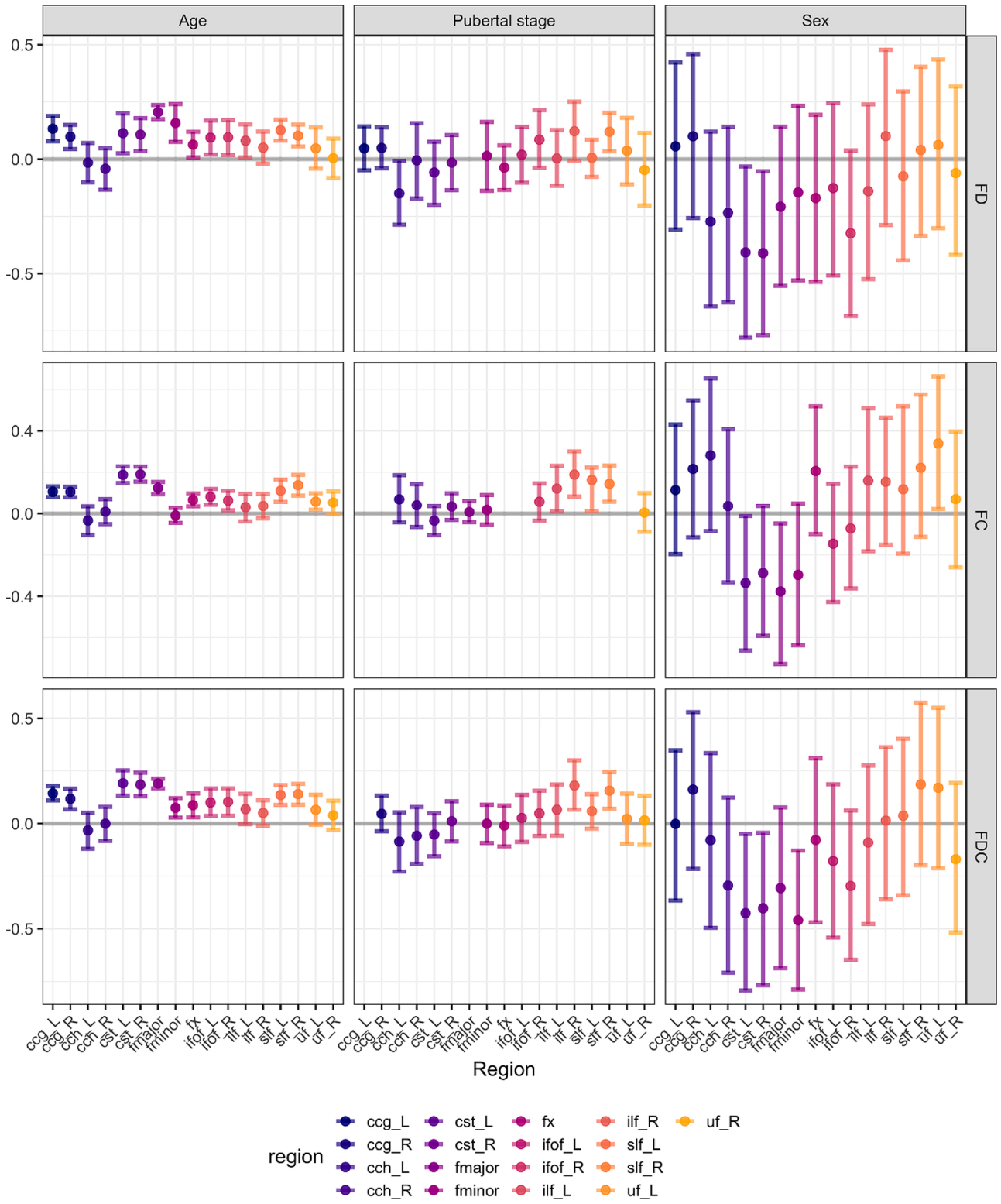

Fig. 3. Relationships between participant characteristics and fibre microstructure across all white matter tracts. 95 % confidence intervals which do not cross zero suggest a relationship between a predictor and FBA metric.

morphology in the right ILF. MD is sensitive to isotropic diffusion in the extracellular space, therefore any increases in intra-axonal signal fraction (proportional to our measure of fibre density) can be reflected by decreases in MD, assuming myelin thickness does not change considerably.

A recent longitudinal study of non-human primate (marmoset) brain development investigated grey matter and white matter changes over 3–7 time-points across the pre-pubertal, pubertal, and post-pubertal periods (Sawiak et al., 2018). Their results showed that the most dynamically developing white matter tracts in the early-pubertal period are the splenium of the corpus callosum, and ILF. These results are in line with our previous cross-sectional results, whereby fibre density

Table 2
Relationship between white matter microstructure with age, sex, and pubertal stage.

Metric	Region	Model		AIC	Age		Sex		Pubertal stage	
					β (95 % CI)	*pFDR*	β (95 % CI)	*pFDR*	β (95 % CI)	*pFDR*
FD	CCG	L	3	487.93	**.13 [.08, .19]**	< .001	.06 [−.31, .42]	.86	.05 [−.05, .14]	.54
		R	3	474.70	**.10 [.04, .15]**	.002	.10 [−.26, .46]	.75	.05 [−.04, .14]	.50
	CCH	L	3	603.95	−.02 [−.10, .07]	.85	−.27 [−.64, .12]	.32	−.15 [−.29, −.01]	.11
		R	5	614.16	−.04 [−.13, .05]	.54	−.23 [−.63, .14]	.43	−.01 [−.17, .16]	.97
	CST	L	3	596.69	**.11 [.03, .20]**	.04	−.41 [−.78, −.03]	.10	−.06 [−.20, .08]	.57
		R	3	549.74	**.11 [.04, .18]**	.02	−.41 [−.77, −.05]	.09	−.02 [−.14, .11]	.89
	Fmajor		1	428.71	**.21 [.17, .24]**	< .001	−.21 [−.55, .14]	.44	–	
	Fminor		5	580.63	**.16 [.08, .24]**	.002	−.15 [−.53, .23]	.62	.01 [−.14, .16]	.91
	FX		3	500.20	.06 [.01, .12]	.10	−.17 [−.54, .19]	.54	−.04 [−.13, .06]	.62
	IFOF	L	3	564.38	.09 [.02, .17]	.05	−.13 [−.51, .24]	.67	.02 [−.10, .14]	.86
		R	3	566.07	.10 [.02, .17]	.06	−.32 [−.69, .04]	.20	.09 [−.04, .21]	.37
	ILF	L	3	564.88	.08 [.01, .15]	.10	−.14 [−.52, .24]	.63	.01 [−.12, .13]	.98
		R	5	542.20	.05 [−.02, .12]	.32	.10 [−.29, .48]	.77	.12 [−.01, .25]	.18
	SLF	L	3	449.63	**.13 [.08, .17]**	< .001	−.07 [−.44, .30]	.82	.01 [−.08, .08]	.95
		R	3	459.20	**.10 [.06, .15]**	< .001	.04 [−.34, .40]	.90	**.12 [.03, .20]**	.03
	UF	L	3	608.60	.05 [−.04, .14]	.51	.06 [−.30, .44]	.86	.04 [−.11, .18]	.77
		R	4	599.97	.01 [−.08, .09]	.96	−.06 [−.42, .32]	.86	−.05 [−.20, .11]	.72
FC	CCG	L	1	328.39	**.11 [.08, .13]**	< .001	.11 [−.20, .43]	.64	–	
		R	1	334.71	**.10 [.08, .13]**	< .001	.22 [−.11, .55]	.39	–	
	CCH	L	3	525.04	−.03 [−.10, .03]	.54	.28 [−.08, .65]	.30	.07 [−.04, .19]	.44
		R	3	491.79	.01 [−.05, .07]	.87	.04 [−.33, .41]	.91	.04 [−.06, .14]	.62
	CST	L	3	358.03	**.19 [.15, .23]**	< .001	−.34 [−.66, −.01]	.12	−.03 [−.10, .04]	.54
		R	3	334.06	**.19 [.15, .23]**	< .001	−.29 [−.59, .04]	.19	.03 [−.03, .10]	.52
	Fmajor		3	301.22	**.12 [.09, .15]**	< .001	−.38 [−.73, −.05]	.11	.01 [−.04, .06]	.87
	Fminor		5	327.30	−.01 [−.05, .03]	.78	−.30 [−.64, .05]	.20	.02 [−.05, .09]	.78
	FX		1	374.13	**.07 [.03, .10]**	< .001	.21 [−.10, .52]	.39	–	
	IFOF	L	1	390.58	**.08 [.04, .12]**	< .001	−.15 [−.43, .14]	.53	–	
		R	5	357.94	**.06 [.02, .11]**	.04	−.07 [−.36, .23]	.78	.06 [−.03, .15]	.41
	ILF	L	3	493.81	.03 [−.04, .10]	.54	.16 [−.18, .51]	.54	.12 [.01, .23]	.10
		R	5	429.17	.04 [−.02, .10]	.43	.15 [−.15, .46]	.54	**.19 [.08, .30]**	.006
	SLF	L	5	442.67	**.11 [.06, .16]**	< .001	.12 [−.19, .52]	.54	.16 [.01, .22]	.10
		R	3	428.74	**.14 [.09, .19]**	< .001	.22 [−.11, .57]	.41	**.14 [.06, .23]**	.009
	UF	L	1	445.80	.06 [.02, .10]	.03	.34 [.02, .66]	.11	–	
		R	3	431.13	.05 [−.01, .11]	.16	.07 [−.26, .40]	.81	.01 [−.09, .10]	.97
FDC	CCG	L	1	427.43	**.14 [.11, .18]**	< .001	−.01 [−.37, .35]	.99	–	
		R	3	437.83	**.12 [.07, .17]**	< .001	.16 [−.22, .53]	.56	.05 [−.04, .13]	.49
	CCH	L	3	604.84	−.03 [−.12, .05]	.62	−.08 [−.50, .33]	.84	−.09 [−.23, .05]	.43
		R	3	582.06	−.01 [−.08, .08]	.99	−.29 [−.71, .12]	.32	−.06 [−.19, .08]	.55
	CST	L	3	490.99	**.19 [.13, .25]**	< .001	−.43 [−.79, −.05]	.09	−.05 [−.16, .05]	.54
		R	3	468.85	**.18 [.13, .24]**	< .001	−.40 [−.77, −.04]	.10	.01 [−.08, .11]	.90
	Fmajor		1	338.21	**.19 [.17, .21]**	< .001	−.31 [−.69, .08]	.26	–	
	Fminor		5	384.20	**.07 [.03, .12]**	.01	**−.46 [−.79, −.13]**	.03	−.01 [−.09, .09]	.99
	FX		3	482.25	**.09 [.03, .14]**	.02	−.08 [−.47, .31]	.82	−.01 [−.11, .09]	.91
	IFOF	L	3	505.27	**.10 [.04, .17]**	.02	−.18 [−.54, .19]	.54	.03 [−.09, .14]	.78
		R	3	489.83	**.10 [.04, .17]**	.01	−.30 [−.65, .06]	.23	.05 [−.06, .16]	.54
	ILF	L	3	536.65	.07 [−.01, .14]	.16	−.09 [−.48, .28]	.78	.07 [−.06, .19]	.49
		R	5	476.66	.05 [−.01, .11]	.26	.01 [−.36, .36]	.97	**.18 [.07, .30]**	.02
	SLF	L	3	432.95	.14 [.09, .18]	< .001	.04 [−.34, .40]	.91	.06 [−.02, .14]	.32
		R	3	451.14	.14 [.09, .19]	< .001	.19 [−.20, .57]	.54	**.16 [.07, .24]**	.003
	UF	L	3	540.59	.07 [−.01, .14]	.19	.17 [−.21, .55]	.55	.02 [−.10, .14]	.84
		R	3	515.73	.04 [−.03, .11]	.49	−.17 [−.52, .19]	.54	.02 [−.10, .13]	.88

Note: Best model fit was determined using the lowest AIC for all models tested within each region (see Table S1 for full model details). Total intracranial volume (TIV) was entered as a covariate for morphological measures (FC, FDC). Abbreviations: CCG = cingulum cingulate gyrus; CCH = cingulum hippocampus; CST = Cortico-spinal tract; FA = Fractional anisotropy; FC = Fibre cross-section; FD = Fibre density; Fmajor = Forceps major; Fminor = Forceps minor; FX = fornix; L = Left; IFOF = inferior fronto-occipital fasciculus; ILF = inferior longitudinal fasciculus; R = Right; SLF = Superior longitudinal fasciculus; UF = uncinate fasciculus. P-values were adjusted for false-discovery rate (p_{FDR}), where bold values denote $p_{FDR} < .05$.

appears to be increasing in the splenium in response to pubertal onset (Genc et al., 2017), and with the current results as we observed increasing fibre morphology in the right ILF with pubertal stage. During the pubertal period, regions experiencing most marked white matter tract thickening were localised to the SLF (Sawiak et al., 2018), consistent with evidence that the SLF does not reach full maturation until the post-pubertal stage (Ladouceur et al., 2012). Overall, we have replicable evidence that the splenium of the corpus callosum and right inferior longitudinal fasciculus are sensitive to pubertal timing, and the right superior longitudinal fasciculus is sensitive to pubertal stage. These findings additionally highlight the sensitivity of advanced microstructural metrics such as fibre density and morphology, as they appear to be sensitive to region-specific white matter changes mediated by pubertal stage.

4.3. Longitudinal change in pubertal stage

We observed that relatively older children with a larger change in PDSS score experienced larger increases in fibre density in the left corticospinal tract, left inferior fronto-occipital fasciculus, left inferior longitudinal fasciculus, and left uncinate fasciculus over the 16-month follow-up period. This may suggest that these left-lateralised association tracts (e.g. IFOF, ILF, UF) with known protracted development in late adolescence (Von Der Heide et al., 2013) are developing at a later age, or 'catching up', in older children with greater increases in pubertal stage. As this association was not predicted apriori, replication of these

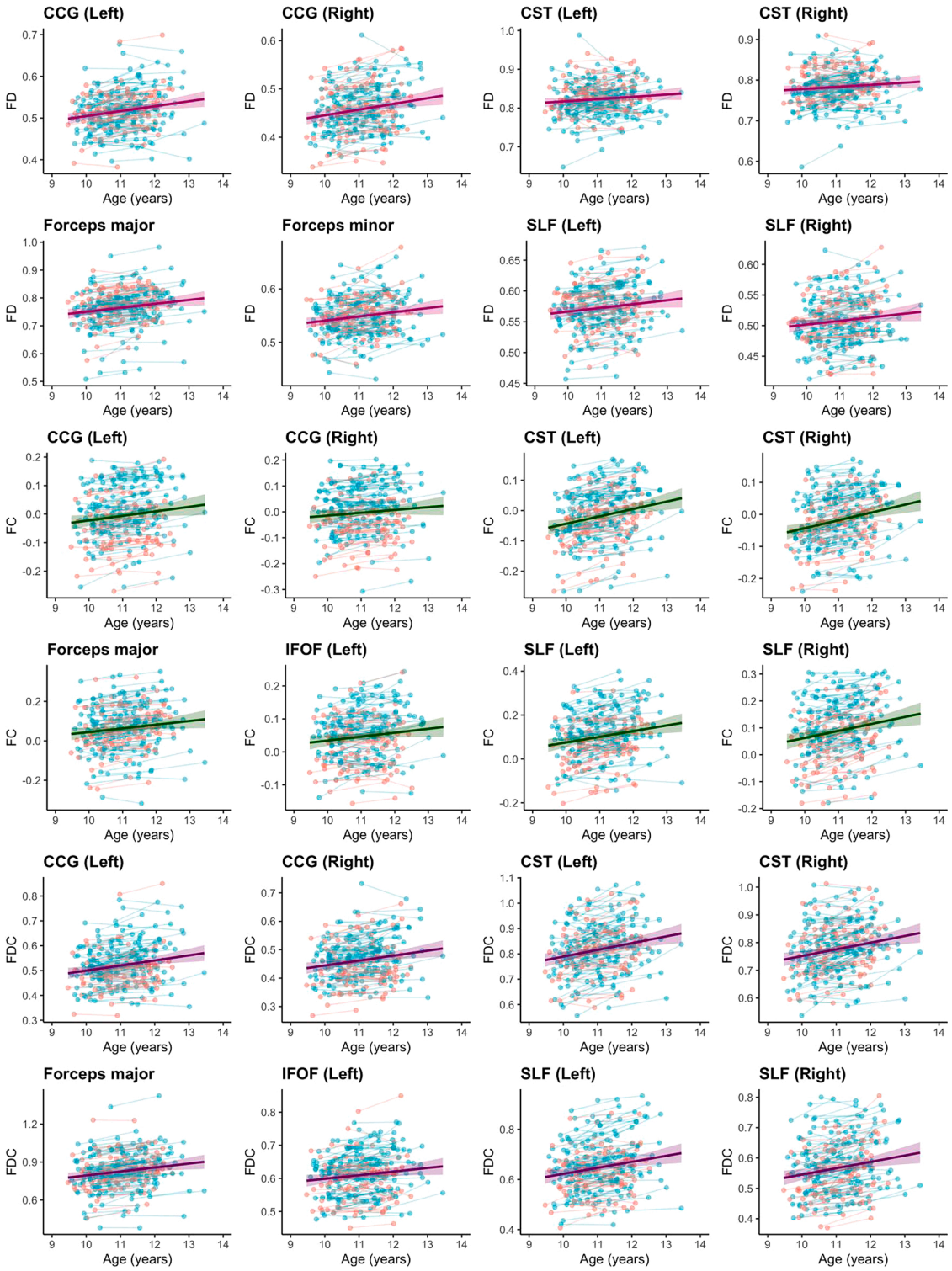

Fig. 4. Longitudinal change in white matter fibre properties for regions with significant age-related increases over time. Blue = boys, Red = girls (For interpretation of the references to colour in this figure legend, the reader is referred to the web version of this article).

findings is required to ensure the stability of these associations.

In a similar aged sample, Ho et al. (2020) revealed that the longitudinal change in testosterone levels in females was related to FA change in the corpus callosum, cingulum cingulate gyrus, and corticospinal tract. Although we did not observe any discernible relationship between the change in fibre density and change in pubertal stage (or sex interactions), differences in analysis approaches (DTI vs. fixel-based metrics) or pubertal staging methods (hormone sampling vs. PDS questionnaire) may reconcile differences between results. Future work should combine fixel-based metrics derived from high b-values with improved pubertal phenotyping to demonstrate replicable evidence of tract-specific microstructural development with respect to puberty.

4.4. Relationship with brain volume

Fibre cross-section is inherently a morphological measure of the

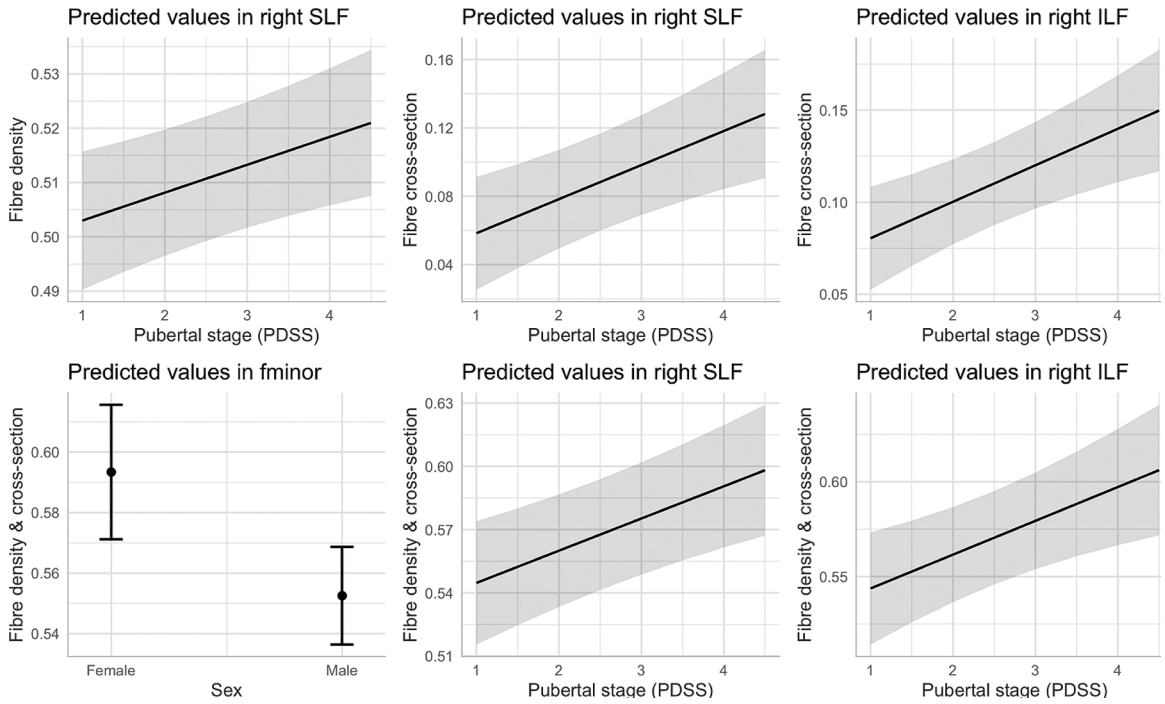

Fig. 5. Marginal effects plots of FBA metrics for sex and pubertal stage.

macroscopic change in cross-sectional area perpendicular to a fibre bundle experienced during registration to a template image (Raffelt et al., 2017). This finding is of special interest to users of the fixel-based analysis framework and derived metrics, as any variable associated with total intracranial volume can potentially conflate interpretations on changes in fibre cross-section (Smith et al., 2019). For example, it is known that on average (for a given age), males have greater intracranial volume than females. Without adjusting for this confound in analyses of fibre cross-section, sex differences could be attributed to biologically relevant differences, when in fact the differences may purely due to large-scale anatomical differences in head size (Luders et al., 2014). Similar patterns were observed in the analyses of fibre density and cross-section, given that this metric is calculated from fibre cross-section. Therefore, the main message of these results, are that these metrics must be interpreted with caution, and that analyses involving morphological measures should be adjusted appropriately for intracranial volume.

4.5. Limitations and future directions

Our measures of symptom severity may be biased as our sample inherently includes children which have either met or not met criteria for ADHD three years prior to neuroimaging. Although our community-based sample captures a wide range of symptom severity for attentional difficulties, our sample is not randomly selected and potentially biased we may be missing out on high-risk children which fit 'in-between' these two ends of the spectrum of symptom severity. Whilst we did not observe a significant relationship between ADHD symptom severity and white matter fibre density (Table S3), future studies should perform larger population-level analyses to account for a wider dimensional range in attentional difficulties.

Our approach studied separate white matter pathways to determine the best fitting model for each region. Whilst useful for ensuring each region is studied with the appropriate predictors, the problem of multiple comparisons can influence the interpretability of results. Dimensionality reduction methods such as principal components analysis (Chamberland et al., 2019; Geeraert et al., 2020) or canonical correlation analysis (Ball et al., 2018) has proven useful in these scenarios, in order to capture components of microstructural attributes which vary together over development.

Finally, we have attempted to mitigate for motion artefact with the use of frame-wise displacement as a covariate, which did not appear to influence the main results. However, robust measures such as temporal signal-to-noise ratio (TSNR) may be more appropriate descriptors of motion artefact (Roalf et al., 2016).

4.6. Conclusion

We summarise our longitudinal findings with four important conclusions: (1) white matter development over the ages of 9–13 years involves dynamic increases in fibre density and morphology in a large range of developmentally-sensitive pathways, (2) pubertal stage is positively associated with fibre density and morphology in the right superior longitudinal fasciculus and fibre morphology in the right inferior fronto-occipital fasciculus, (3) intra-cranial volume is highly predictive of fibre morphology and should be modelled appropriately, and (4) the longitudinal change in fibre density is associated with the change in pubertal stage in relatively older children. These results shed light on key white matter fibre-specific properties with age, sex and pubertal development across childhood and adolescence.

Declaration of Competing Interest

All authors declare no real or potential conflicts of interest.

Acknowledgements

Data used in the preparation of this article were obtained from the NICAP study (National Health and Medical Research Council (NHMRC); project grant #1065895). The research and analyses were conducted within the Developmental Imaging research group, Murdoch Children's Research Institute, supported by the Victorian Government's Operational Infrastructure Support Program, and The Royal Children's Hospital Foundation devoted to raising funds for research at The Royal Children's Hospital. SG was supported by an Australian Government Research Training Program (RTP) scholarship. ES was supported by an

NHMRC Career Development Award (1110688).

We extend our gratitude to the families that have participated for a number of years in this longitudinal study. We thank Michael Kean and The Royal Children's Hospital Medical Imaging staff for their assistance and expertise in the collection of the MRI data included in this study.

Appendix A. Supplementary data

Supplementary material related to this article can be found, in the online version, at doi:https://doi.org/10.1016/j.dcn.2020.100853.

References

Andersson, J.L.R., Sotiropoulos, S.N., 2016. An integrated approach to correction for off-resonance effects and subject movement in diffusion MR imaging. Neuroimage 125, 1063–1078. https://doi.org/10.1016/j.neuroimage.2015.10.019.

Bach, M., Laun, F.B., Leemans, A., Tax, C.M., Biessels, G.J., Stieltjes, B., Maier-Hein, K.H., 2014. Methodological considerations on tract-based spatial statistics (TBSS). Neuroimage 100, 358–369. https://doi.org/10.1016/j.neuroimage.2014.06.021.

Ball, G., Malpas, C.B., Genc, S., Efron, D., Sciberras, E., Anderson, V., Nicholson, J.M., Silk, T.J., 2018. Multimodal structural neuroimaging markers of brain development and ADHD symptoms. Am. J. Psychiatry 0 (0). https://doi.org/10.1176/appi.ajp.2018.18010034 appiajp201818010034.

Bates, D., Mächler, M., Bolker, B., Walker, S., 2015. Fitting linear mixed-effects models using lme4. J. Stat. Softw. 1 (1) https://doi.org/10.18637/jss.v067.i01 (2015).

Beaulieu, C., 2009. The biological basis of diffusion anisotropy. Diffusion Mri: From Quantitative Measurement to in Vivo Neuroanatomy, pp. 105–126. https://doi.org/10.1016/B978-0-12-374709-9.00006-7.

Benjamini, Y., Hochberg, Y., 1995. Controlling the false discovery rate: a practical and powerful approach to multiple testing. J. R. Stat. Soc. Ser. B 57 (1), 289–300.

Brouwer, R.M., Mandl, R.C., Schnack, H.G., van Soelen, I.L., van Baal, G.C., Peper, J.S., Kahn, R.S., Boomsma, D.I., Hulshoff Pol, H.E., 2012. White matter development in early puberty: a longitudinal volumetric and diffusion tensor imaging twin study. PLoS One 7 (4), e32316.

Catani, M., Jones, D.K., ffytche, D.H., 2005. Perisylvian language networks of the human brain. Ann. Neurol. 57 (1), 8–16. https://doi.org/10.1002/ana.20319.

Chamberland, M., Raven, E.P., Genc, S., Duffy, K., Descoteaux, M., Parker, G.D., Tax, C.M.W., Jones, D.K., 2019. Dimensionality reduction of diffusion MRI measures for improved tractometry of the human brain. Neuroimage 200, 89–100. https://doi.org/10.1016/j.neuroimage.2019.06.020.

Conners, C.K., Pitkanen, J., Rzepa, S.R., 2011. Conners 3rd edition (Conners 3; Conners 2008). In: Kreutzer, J.S., DeLuca, J., Caplan, B. (Eds.), Encyclopedia of Clinical Neuropsychology. Springer New York, New York, NY, pp. 675–678. https://doi.org/10.1007/978-0-387-79948-3_1534.

Dorn, L.D., Dahl, R.E., Woodward, H.R., Biro, F., 2006. Defining the boundaries of early adolescence: a user's guide to assessing pubertal status and pubertal timing in research with adolescents. Appl. Dev. Sci. 10 (1), 30–56. https://doi.org/10.1207/s1532480xads1001_3.

Genc, S., Seal, M.L., Dhollander, T., Malpas, C.B., Hazell, P., Silk, T.J., 2017. White matter alterations at pubertal onset. Neuroimage 156, 286–292. https://doi.org/10.1016/j.neuroimage.2017.05.017.

Genc, S., Smith, R.E., Malpas, C.B., Anderson, V., Nicholson, J.M., Efron, D., Sciberras, E., Seal, M.L., Silk, T.J., 2018. Development of white matter fibre density and morphology over childhood: a longitudinal fixel-based analysis. Neuroimage 183, 666–676. https://doi.org/10.1016/j.neuroimage.2018.08.043.

Genc, S., Tax, C.M.W., Raven, E.P., Chamberland, M., Parker, G.D., Jones, D.K., 2020. Impact of b-value on estimates of apparent fibre density. Hum. Brain Mapp. https://doi.org/10.1002/hbm.24964, 2020.2001.2015.905802.

Geeraert, B.L., Chamberland, M., Lebel, R.M., Lebel, C., 2020. Multimodal principal component analysis to identify major features of white matter structure and links to reading. PLOS ONE 15 (8), e0233244.

Goodman, R., 1997. The strengths and difficulties questionnaire: a research note. J. Child Psychol. Psychiatry 38 (5), 581–586. https://doi.org/10.1111/j.1469-7610.1997.tb01545.x.

Goodman, A., Lamping, D.L., Ploubidis, G.B., 2010. When to use broader internalising and externalising subscales instead of the hypothesised five subscales on the Strengths and Difficulties Questionnaire (SDQ): data from British parents, teachers and children. J. Abnorm. Child Psychol. 38 (8), 1179–1191. https://doi.org/10.1007/s10802-010-9434-x.

Herting, M.M., Maxwell, E.C., Irvine, C., Nagel, B.J., 2012. The impact of sex, puberty, and hormones on white matter microstructure in adolescents. Cereb. Cortex 22 (9), 1979–1992. https://doi.org/10.1093/cercor/bhr246.

Herting, M.M., Gautam, P., Spielberg, J.M., Kan, E., Dahl, R.E., Sowell, E.R., 2014. The role of testosterone and estradiol in brain volume changes across adolescence: a longitudinal structural MRI study. Hum. Brain Mapp. 35 (11), 5633–5645. https://doi.org/10.1002/hbm.22575.

Herting, M.M., Kim, R., Uban, K.A., Kan, E., Binley, A., Sowell, E.R., 2017. Longitudinal changes in pubertal maturation and white matter microstructure. Psychoneuroendocrinology 81, 70–79. https://doi.org/10.1016/j.psyneuen.2017.03.017.

Ho, T.C., Colich, N.L., Sisk, L.M., Oskirko, K., Jo, B., Gotlib, I.H., 2020. Sex differences in the effects of gonadal hormones on white matter microstructure development in adolescence. Dev. Cogn. Neurosci. 42, 100773 https://doi.org/10.1016/j.dcn.2020.100773.

Jones, D.K., Knosche, T.R., Turner, R., 2013. White matter integrity, fiber count, and other fallacies: the do's and don'ts of diffusion MRI. Neuroimage 73, 239–254. https://doi.org/10.1016/j.neuroimage.2012.06.081.

Juraska, J.M., Willing, J., 2017. Pubertal onset as a critical transition for neural development and cognition. Brain Res. 1654 (Pt B), 87–94. https://doi.org/10.1016/j.brainres.2016.04.012.

Kelley, S., Plass, J., Bender, A.R., Polk, T.A., 2019. Age-related differences in white matter: comparing fixel based and tensor based analyses. bioRxiv. https://doi.org/10.1101/751628, 751628.

Kessler, R.C., Berglund, P., Demler, O., Jin, R., Merikangas, K.R., Walters, E.E., 2005. Lifetime prevalence and age-of-onset distributions of DSM-IV disorders in the National Comorbidity Survey Replication. Arch. Gen. Psychiatry 62 (6), 593–602. https://doi.org/10.1001/archpsyc.62.6.593.

Krogsrud, S.K., Fjell, A.M., Tamnes, C.K., Grydeland, H., Mork, L., Due-Tonnessen, P., Bjornerud, A., Sampaio-Baptista, C., Andersson, J., Johansen-Berg, H., Walhovd, K. B., 2016. Changes in white matter microstructure in the developing brain–A longitudinal diffusion tensor imaging study of children from 4 to 11years of age. Neuroimage 124 (Pt A), 473–486.

Ladouceur, C.D., Peper, J.S., Crone, E.A., Dahl, R.E., 2012. White matter development in adolescence: the influence of puberty and implications for affective disorders. Dev. Cogn. Neurosci. 2 (1), 36–54. https://doi.org/10.1016/j.dcn.2011.06.002.

Langberg, J.M., Epstein, J.N., Altaye, M., Molina, B.S.G., Arnold, L.E., Vitiello, B., 2008. The transition to middle school is associated with changes in the developmental trajectory of ADHD symptomatology in young adolescents with ADHD. J. Clin. Child Adolesc. Psychol. 53 37 (3), 651–663. https://doi.org/10.1080/15374410802148095. American Psychological Association, Division.

Lebel, C., Beaulieu, C., 2011. Longitudinal development of human brain wiring continues from childhood into adulthood. J. Neurosci. 31 (30), 10937–10947. https://doi.org/10.1523/JNEUROSCI.5302-10.2011.

Luders, E., Toga, A.W., Thompson, P.M., 2014. Why size matters: differences in brain volume account for apparent sex differences in callosal anatomy: the sexual dimorphism of the corpus callosum. Neuroimage 84, 820–824. https://doi.org/10.1016/j.neuroimage.2013.09.040.

M, A., D, P., K, W., Marshall, T.R., Kievit, R.A., 2019. Raincloud plots: a multi-platform tool for robust data visualization. Wellcome Open Res. https://doi.org/10.12688/wellcomeopenres.15191.1.

Maninger, N., Wolkowitz, O.M., Reus, V.I., Epel, E.S., Mellon, S.H., 2009. Neurobiological and neuropsychiatric effects of dehydroepiandrosterone (DHEA) and DHEA sulfate (DHEAS). Front. Neuroendocrinol. 30 (1), 65–91. https://doi.org/10.1016/j.yfrne.2008.11.002.

Menzies, L., Goddings, A.L., Whitaker, K.J., Blakemore, S.J., Viner, R.M., 2015. The effects of puberty on white matter development in boys. Dev. Cogn. Neurosci. 11, 116–128. https://doi.org/10.1016/j.dcn.2014.10.002.

Pangelinan, M.M., Leonard, G., Perron, M., Pike, G.B., Richer, L., Veillette, S., Pausova, Z., Paus, T., 2016. Puberty and testosterone shape the corticospinal tract during male adolescence. Brain Struct. Funct. 221 (2), 1083–1094. https://doi.org/10.1007/s00429-014-0956-9.

Paus, T., Keshavan, M., Giedd, J.N., 2008. Why do many psychiatric disorders emerge during adolescence? Nat. Rev. Neurosci. 9 (12), 947–957. https://doi.org/10.1038/nrn2513.

Perrin, J.S., Herve, P.Y., Leonard, G., Perron, M., Pike, G.B., Pitiot, A., Richer, L., Veillette, S., Pausova, Z., Paus, T., 2008. Growth of white matter in the adolescent brain: role of testosterone and androgen receptor. J. Neurosci. 28 (38), 9519–9524. https://doi.org/10.1523/JNEUROSCI.1212-08.2008.

Pesaresi, M., Soon-Shiong, R., French, L., Kaplan, D.R., Miller, F.D., Paus, T., 2015. Axon diameter and axonal transport: in vivo and in vitro effects of androgens. Neuroimage 115, 191–201. https://doi.org/10.1016/j.neuroimage.2015.04.048.

Petersen, A.C., Crockett, L., Richards, M., Boxer, A., 1988. A self-report measure of pubertal status: reliability, validity, and initial norms. J. Youth Adolesc. 17 (2), 117–133. https://doi.org/10.1007/BF01537962.

Pines, A.R., Cieslak, M., Larsen, B., Baum, G.L., Cook, P.A., Adebimpe, A., Dávila, D.G., Elliott, M.A., Jirsaraie, R., Murtha, K., Oathes, D.J., Piiwaa, K., Rosen, A.F.G., Rush, S., Shinohara, R.T., Bassett, D.S., Roalf, D.R., Satterthwaite, T.D., 2020. Leveraging multi-shell diffusion for studies of brain development in youth and young adulthood. Dev. Cogn. Neurosci. https://doi.org/10.1016/j.dcn.2020.100788, 100788.

Polanczyk, G., de Lima, M.S., Horta, B.L., Biederman, J., Rohde, L.A., 2007. The worldwide prevalence of ADHD: a systematic review and metaregression analysis. Am. J. Psychiatry 164 (6), 942–948. https://doi.org/10.1176/ajp.2007.164.6.942.

Raffelt, D., Tournier, J.D., Fripp, J., Crozier, S., Connelly, A., Salvado, O., 2011. Symmetric diffeomorphic registration of fibre orientation distributions. Neuroimage 56 (3), 1171–1180. https://doi.org/10.1016/j.neuroimage.2011.02.014.

Raffelt, D.A., Smith, R.E., Ridgway, G.R., Tournier, J.D., Vaughan, D.N., Rose, S., Henderson, R., Connelly, A., 2015. Connectivity-based fixel enhancement: whole-brain statistical analysis of diffusion MRI measures in the presence of crossing fibres. Neuroimage 117, 40–55. https://doi.org/10.1016/j.neuroimage.2015.05.039.

Raffelt, D.A., Tournier, J.D., Smith, R.E., Vaughan, D.N., Jackson, G., Ridgway, G.R., Connelly, A., 2017. Investigating white matter fibre density and morphology using fixel-based analysis. Neuroimage 144 (Pt A), 58–73. https://doi.org/10.1016/j.neuroimage.2016.09.029.

Reuter, M., Schmansky, N.J., Rosas, H.D., Fischl, B., 2012. Within-subject template estimation for unbiased longitudinal image analysis. Neuroimage 61 (4), 1402–1418. https://doi.org/10.1016/j.neuroimage.2012.02.084.

Roalf, D.R., Quarmley, M., Elliott, M.A., Satterthwaite, T.D., Vandekar, S.N., Ruparel, K., Gennatas, E.D., Calkins, M.E., Moore, T.M., Hopson, R., Prabhakaran, K., Jackson, C. T., Verma, R., Hakonarson, H., Gur, R.C., Gur, R.C.E., 2016. The impact of quality assurance assessment on diffusion tensor imaging outcomes in a large-scale population-based cohort. Neuroimage 125, 903–919. https://doi.org/10.1016/j.neuroimage.2015.10.068.

Sawiak, S.J., Shiba, Y., Oikonomidis, L., Windle, C.P., Santangelo, A.M., Grydeland, H., Cockcroft, G., Bullmore, E.T., Roberts, A.C., 2018. Trajectories and milestones of cortical and subcortical development of the marmoset brain from infancy to adulthood. Cereb. Cortex 28 (12), 4440–4453. https://doi.org/10.1093/cercor/bhy256.

Schmithorst, V.J., Holland, S.K., Dardzinski, B.J., 2008. Developmental differences in white matter architecture between boys and girls. Hum. Brain Mapp. 29 (6), 696–710. https://doi.org/10.1002/hbm.20431.

Sciberras, E., Efron, D., Schilpzand, E.J., Anderson, V., Jongeling, B., Hazell, P., Ukoumunne, O.C., Nicholson, J.M., 2013. The Children's Attention Project: a community-based longitudinal study of children with ADHD and non-ADHD controls. BMC Psychiatry 13, 18. https://doi.org/10.1186/1471-244X-13-18.

Seunarine, K.K., Clayden, J.D., Jentschke, S., Munoz, M., Cooper, J.M., Chadwick, M.J., Banks, T., Vargha-Khadem, F., Clark, C.A., 2016. Sexual dimorphism in white matter developmental trajectories using tract-based spatial statistics. Brain Connect. 6 (1), 37–47. https://doi.org/10.1089/brain.2015.0340.

Shankman, S.A., Lewinsohn, P.M., Klein, D.N., Small, J.W., Seeley, J.R., Altman, S.E., 2009. Subthreshold conditions as precursors for full syndrome disorders: a 15-year longitudinal study of multiple diagnostic classes. J. Child Psychol. Psychiatry 50 (12), 1485–1494. https://doi.org/10.1111/j.1469-7610.2009.02117.x.

Shirtcliff, E.A., Dahl, R.E., Pollak, S.D., 2009. Pubertal development: correspondence between hormonal and physical development. Child Dev. 80 (2), 327–337. https://doi.org/10.1111/j.1467-8624.2009.01263.x.

Silk, T.J., Genc, S., Anderson, V., Efron, D., Hazell, P., Nicholson, J.M., Kean, M., Malpas, C.B., Sciberras, E., 2016. Developmental brain trajectories in children with ADHD and controls: a longitudinal neuroimaging study. BMC Psychiatry 16, 59. https://doi.org/10.1186/s12888-016-0770-4.

Sisk, C.L., Foster, D.L., 2004. The neural basis of puberty and adolescence. Nat. Neurosci. 7 (10), 1040–1047. https://doi.org/10.1038/nn1326.

Smith, S.M., Jenkinson, M., Woolrich, M.W., Beckmann, C.F., Behrens, T.E., Johansen-Berg, H., Bannister, P.R., De Luca, M., Drobnjak, I., Flitney, D.E., Niazy, R.K., Saunders, J., Vickers, J., Zhang, Y., De Stefano, N., Brady, J.M., Matthews, P.M., 2004. Advances in functional and structural MR image analysis and implementation as FSL. Neuroimage 23 (Suppl. 1), S208–219. https://doi.org/10.1016/j.neuroimage.2004.07.051.

Smith, R., Dhollander, T., Connelly, A., 2019. On the regression of intracranial volume in fixel-based analysis. 3385. Proc. Intl. Soc. Mag. Reson. Med. ISMRM, Montreal, Canada.

Tamnes, C.K., Ostby, Y., Fjell, A.M., Westlye, L.T., Due-Tonnessen, P., Walhovd, K.B., 2010. Brain maturation in adolescence and young adulthood: regional age-related changes in cortical thickness and white matter volume and microstructure. Cereb Cortex 20 (3), 534–548.

Tamnes, C.K., Roalf, D.R., Goddings, A.L., Lebel, C., 2017. Diffusion MRI of white matter microstructure development in childhood and adolescence: methods, challenges and progress. Dev. Cogn. Neurosci. https://doi.org/10.1016/j.dcn.2017.12.002.

Tamnes, C.K., Roalf, D.R., Goddings, A.-L., Lebel, C., 2018. Diffusion MRI of white matter microstructure development in childhood and adolescence: methods, challenges and progress. Dev. Cogn. Neurosci. 33, 161–175. https://doi.org/10.1016/j.dcn.2017.12.002.

Tournier, J.D., Smith, R., Raffelt, D., Tabbara, R., Dhollander, T., Pietsch, M., Christiaens, D., Jeurissen, B., Yeh, C.-H., Connelly, A., 2019. MRtrix3: a fast, flexible and open software framework for medical image processing and visualisation. Neuroimage 202, 116137. https://doi.org/10.1016/j.neuroimage.2019.116137.

Tustison, N.J., Avants, B.B., Cook, P.A., Zheng, Y., Egan, A., Yushkevich, P.A., Gee, J.C., 2010. N4ITK: improved N3 bias correction. IEEE Trans. Med. Imaging 29 (6), 1310–1320. https://doi.org/10.1109/TMI.2010.2046908.

van Langen, J., 2020. Open-visualizations for Repeated Measures in R. https://github.com/jorvlan/open-visualizations.

Veraart, J., Fieremans, E., Novikov, D.S., 2016. Diffusion MRI noise mapping using random matrix theory. Magn. Reson. Med. 76 (5), 1582–1593. https://doi.org/10.1002/mrm.26059.

Von Der Heide, R.J., Skipper, L.M., Klobusicky, E., Olson, I.R., 2013. Dissecting the uncinate fasciculus: disorders, controversies and a hypothesis. Brain 136 (Pt 6), 1692–1707. https://doi.org/10.1093/brain/awt094.

Wakana, S., Caprihan, A., Panzenboeck, M.M., Fallon, J.H., Perry, M., Gollub, R.L., Hua, K., Zhang, J., Jiang, H., Dubey, P., Blitz, A., van Zijl, P., Mori, S., 2007. Reproducibility of quantitative tractography methods applied to cerebral white matter. Neuroimage 36 (3), 630–644. https://doi.org/10.1016/j.neuroimage.2007.02.049.

Wechsler, D., 1999. Wechsler Abbreviated Scale of Intelligence. The Psychological Corporation: Harcourt Brace & Company, New York, NY.

Wickham, H., 2016. ggplot2: Elegant Graphics for Data Analysis. Springer-Verlag, New York. https://ggplot2.tidyverse.org.

Zhang, Z., Cerghet, M., Mullins, C., Williamson, M., Bessert, D., Skoff, R., 2004. Comparison of in vivo and in vitro subcellular localization of estrogen receptors alpha and beta in oligodendrocytes. J. Neurochem. 89 (3), 674–684. https://doi.org/10.1111/j.1471-4159.2004.02388.x.